MULTILAYER GRAPHENE

I. SCALES OF THE HAMILTONIAN

We set $\hbar = 1$ throughout all the text. The UV cutoff $\mathcal{K}$ of the system, fixed by the lattice parameter $2\pi/\mathcal{K}$, provides us a natural scale to measure the momenta, such that any momentum index $\mathbf{k}$ is normalized by $\mathcal{K}$. In this way, we get the kinetic non-interacting Hamiltonian

$$H_{\text{kin}} = E_{\text{UV}} \sum_{\mathbf{k}\sigma\sigma'} \left(\frac{|\mathbf{k}|}{\mathcal{K}}\right)^m \psi^\dagger_{\mathbf{k},\sigma} \left(\hat{\mathbf{k}}_m \cdot \boldsymbol{\sigma}_{\sigma\sigma'}\right) \psi_{\mathbf{k},\sigma'}, \quad (1)$$

where $[\hat{\mathbf{k}}_m] = \big(\cos(m\phi_m)\ \sin(m\phi_m)\big)$ and E_{UV} is the numerical value of the kinetic term evaluated at $\mathcal{K}$, and whose shape depends on m:

- $m = 1$: $E_{\text{UV}} = v\mathcal{K}$, where v is the Fermi velocity of the Dirac fermions.
- $m = 2$: $E_{\text{UV}} = \mathcal{K}^2/2m_e$, where m_e is the effective mass of the electron.

The potential is given by

$$V_{\mathbf{r}} = V_0 e^{-r^2/2a^2} \quad (2)$$

with V_0 the intensity of the Gaussian potential and a the spreading in the real space. Its Fourier transform is

$$V_{\mathbf{k}} = 2\pi a^2 V_0 e^{-\frac{a^2k^2}{2}} = \frac{E_{\text{UV}}}{\mathcal{K}^2}\left[\frac{2\pi(a\mathcal{K})^2 V_0}{E_{\text{UV}}} e^{-\frac{(a\mathcal{K})^2}{2}\left(\frac{k}{\mathcal{K}}\right)^2}\right],$$

$$V_{\mathbf{k}} = \frac{E_{\text{UV}}}{\mathcal{K}^2}\left(g_0 e^{-\frac{a^2_{\mathcal{K}}}{2}\left(\frac{k}{\mathcal{K}}\right)^2}\right), \quad (3)$$

where $k = |\mathbf{k}|$. It is assumed that $a > 2\pi/\mathcal{K}$, i.e., the spreading of the Gaussian should be larger than the lattice parameter $2\pi/\mathcal{K}$. The additional two nondimensional parameters are:

- Reciprocal spreading $a_{\mathcal{K}} = a\mathcal{K}$: Determines how concentrated is the potential in the reciprocal space. $a_{\mathcal{K}}$ is constrained to be larger than one.
- Coupling constant $g_{\mathcal{K}} = 2\pi a^2_{\mathcal{K}} V_0/E_{\text{UV}}$: Relates the intensity of the Gaussian potential in the reciprocal space with E_{UV}, the kinetic energy at the UV cutoff.

Lastly, the interaction Hamiltonian can be expressed as

$$H_{\text{int}} = \frac{1}{2A}\sum_{\mathbf{k}\mathbf{k}'}\sum_{\sigma\sigma'} V_{\mathbf{q}} \psi^\dagger_{\mathbf{k}'+\mathbf{q},\sigma'} \psi^\dagger_{\mathbf{k}-\mathbf{q},\sigma} \psi_{\mathbf{k},\sigma} \psi_{\mathbf{k}',\sigma'} \quad (4)$$

$$= \frac{E_{\text{UV}}}{2A\mathcal{K}^2}\sum_{\mathbf{k}\mathbf{k}'}\sum_{\sigma\sigma'} g_{\mathcal{K}} e^{-\frac{a^2_{\mathcal{K}}}{2}\left(\frac{k}{\mathcal{K}}\right)^2} \psi^\dagger_{\mathbf{k}'+\mathbf{q},\sigma'} \psi^\dagger_{\mathbf{k}-\mathbf{q},\sigma} \psi_{\mathbf{k},\sigma} \psi_{\mathbf{k}',\sigma'}.$$

where A is the total area of the system.

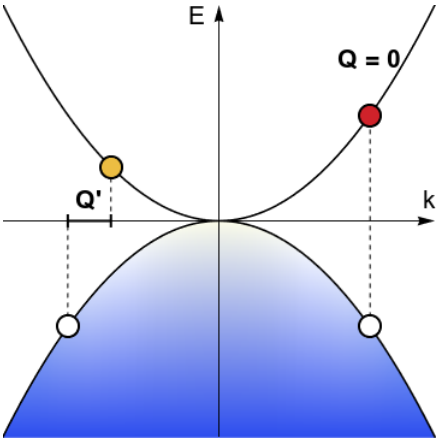

FIG. 1. $\mathbf{Q} = 0$ and $\mathbf{Q} \neq 0$ excitations on the parabolic bands.

II. RESTRICTED HILBERT SPACE FOR $\mathbf{Q} = 0$ EXCITONS AND PSEUDOSPIN BASIS

The optical relevant excitations of the system correspond to the $\mathbf{Q} = 0$ excitons, as shown in FIG. 1. These ones do not modify the momentum label of the electron when it jumps from the valence to the conduction band, and consequently, any interaction between a pair excitons at momenta $\mathbf{k}_1$ and $\mathbf{k}_2$ should only interchange their momentum labels. In other words, by having into account only $\mathbf{Q} = 0$ excitations, the Hilbert space of the system results restricted onto the singly-occupied sites in the momentum lattice. A good operator to describe the singly-occupied constrain is

$$s^\mu_{\mathbf{k}} = \sum_{\sigma\sigma'} \psi^\dagger_{\mathbf{k},\sigma} \sigma^\mu_{\sigma\sigma'} \psi_{\mathbf{k},\sigma'}. \quad (5)$$

where $\sigma^\mu_{\sigma,\sigma'}$ is the component $\sigma\sigma'$ of the matrix σ^μ, given by the generators ot the SU(2) Lie algebra, i.e., the Pauli matrices and the identity

$$\sigma^0 = \begin{pmatrix} 1 & 0 \\ 0 & 1 \end{pmatrix}, \quad \sigma^1 = \begin{pmatrix} 0 & 1 \\ 1 & 0 \end{pmatrix}, \quad \sigma^2 = \begin{pmatrix} 0 & -i \\ i & 0 \end{pmatrix}, \quad \sigma^3 = \begin{pmatrix} 1 & 0 \\ 0 & -1 \end{pmatrix}, \quad (6)$$

The matrix σ^0 is useful to express the singly-occupied condition as the constrain

$$s^0_{\mathbf{k}} = \sum_{\sigma\sigma'} \psi^\dagger_{\mathbf{k},\sigma} \sigma^0_{\sigma\sigma'} \psi_{\mathbf{k},\sigma'} = \sum_{\sigma\sigma'} \psi^\dagger_{\mathbf{k},\sigma} \delta_{\sigma\sigma'} \psi_{\mathbf{k},\sigma'} = \sum_{\sigma\sigma'} \psi^\dagger_{\mathbf{k},\sigma} \psi_{\mathbf{k},\sigma} = \sum_{\sigma} n_{\mathbf{k},\sigma} = 1. \quad (7)$$

.

The following steps show how the four-fermion term in the interacion Hamiltonian can be expressed under the singly-occupied constrain. The completeness relation of the Pauli matrices

$$\sum_{\mu=0}^{3} \sigma^\mu_{\sigma\sigma'} \sigma^\mu_{\tau\tau'} = 2\delta_{\sigma\tau'}\delta_{\sigma'\tau}, \quad (8)$$

and the trace of Pauli matrices bilinears

$$\mathrm{tr}\left(\sigma^{\mu}\sigma^{\mu'}\right)=\sum_{\tau,\tau'}\sigma^{\mu}_{\tau\tau'}\sigma^{\mu'}_{\tau'\tau}=2\delta^{\mu\mu'}, \tag{9}$$

are useful to find the inverse relation between fermion bilinears and Pauli matrices

$$\begin{aligned}\sum_{\mu=0}^{3}\sigma^{\mu}_{\tau\tau'}s^{\mu}_{\mathbf{k}}&=\sum_{\mu=0}^{3}\sum_{\sigma\sigma'}\psi^{\dagger}_{\mathbf{k},\sigma}\sigma^{\mu}_{\sigma\sigma'}\sigma^{\mu}_{\tau,\tau'}\psi_{\mathbf{k},\sigma'}\\&=2\sum_{\sigma\sigma'}\psi^{\dagger}_{\mathbf{k},\sigma}\delta_{\sigma\tau'}\delta_{\sigma'\tau}\psi_{\mathbf{k},\sigma'}\\&=2\psi^{\dagger}_{\mathbf{k},\tau'}\psi_{\mathbf{k},\tau}.\end{aligned} \tag{10}$$

In this way, the fermion bilinears can then be expanded in terms of the generators of the Lie algebra of the group SU(2)

$$\psi^{\dagger}_{\mathbf{k},\tau'}\psi_{\mathbf{k},\tau}=\frac{1}{2}\sum_{\mu=0}^{3}s^{\mu}_{\mathbf{k}}\sigma^{\mu}_{\tau\tau'}, \tag{11}$$

The Eq. (11) is then useful to express the four-fermion term of the interaction Hamiltonian after some anticommutations to match fermion operators that share the same momentum label, such as follows

$$\begin{aligned}&\sum_{\tau,\tau'}\left(\psi^{\dagger}_{\mathbf{k},\tau}\psi_{\mathbf{k},\tau'}\right)\left(\psi^{\dagger}_{\mathbf{k}',\sigma}\psi_{\mathbf{k}',\sigma'}\right)=\\&=\sum_{\tau,\tau'}\left(\frac{1}{2}\sum_{\mu=0}^{3}\sigma^{\mu}_{\tau'\tau}s^{\mu}_{\mathbf{k}}\right)\left(\frac{1}{2}\sum_{\mu'=0}^{3}\sigma^{\mu'}_{\tau\tau'}s^{\mu'}_{\mathbf{k}'}\right)\\&=\frac{1}{4}\sum_{\mu,\mu'}s^{\mu}_{\mathbf{k}}s^{\mu'}_{\mathbf{k}'}\sum_{\tau,\tau'}\sigma^{\mu}_{\tau'\tau}\sigma^{\mu'}_{\tau\tau'}\\&=\frac{1}{4}\sum_{\mu,\mu'}s^{\mu}_{\mathbf{k}}s^{\mu'}_{\mathbf{k}'}\mathrm{tr}\left(\sigma^{\mu}\sigma^{\mu'}\right)\\&=\frac{1}{2}\sum_{\mu,\mu'}s^{\mu}_{\mathbf{k}}s^{\mu'}_{\mathbf{k}'}\delta^{\mu\mu'}=\frac{1}{2}\sum_{\mu,\mu'}s^{\mu}_{\mathbf{k}}s^{\mu}_{\mathbf{k}'}=\frac{1+\mathbf{s}_{\mathbf{k}}\cdot\mathbf{s}_{\mathbf{k}'}}{2}\end{aligned} \tag{12}$$

Consequently, the original fermion Hamiltonian projected onto the singly-occupied is expressed as

$$\begin{aligned}&\mathcal{P}H\mathcal{P}=\\&E_{\mathrm{UV}}\sum_{\mathbf{k}}\left(\frac{|\mathbf{k}|}{\mathcal{K}}\right)^{m}\hat{\mathbf{k}}_{m}\cdot\mathbf{s}_{\mathbf{k}}-\sum_{\mathbf{k}_1\neq\mathbf{k}_2}\frac{V_{\mathbf{k}_1-\mathbf{k}_2}}{4A}\mathbf{s}_{\mathbf{k}_1}\cdot\mathbf{s}_{\mathbf{k}_2},\end{aligned} \tag{13}$$

where the first term represents a m-folded spin vortex (see FIG. 2) and the second term is an effective ferromagnetic exchange.

III. EXPANSION ABOUT THE NON-INTERACTING GROUND STATE

A. Band basis and interaction matrix

In this section, we provide details of the derivation of Eqs. (27) to (29) starting from Eq. (1). We begin

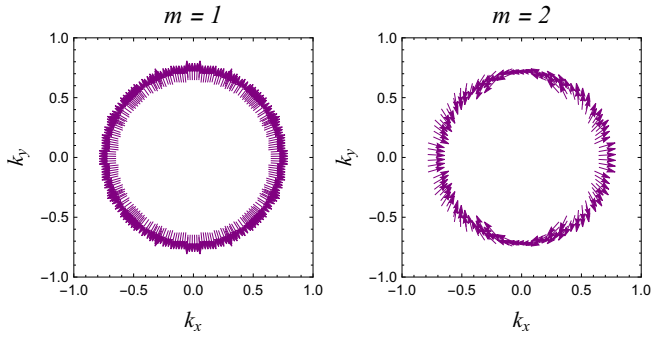

FIG. 2. Polar distribution of the vector $[\hat{\mathbf{k}}_m] = \big(\cos(m\phi_m)\ \sin(m\phi_m)\big)$ used to describe the classical ground state of the system.

describing the transfomation from pseudo-spin basis onto band basis. In the band basis $s=\{+,-\}$ the kinetic term is:

$$\begin{aligned}&\psi^{\dagger}_{\mathbf{k}\sigma}\left(\hat{\mathbf{k}}_m\cdot\boldsymbol{\sigma}_{\sigma\sigma'}\right)\psi_{\mathbf{k}\sigma'}=\\&\quad=e^{-im\phi}\psi^{\dagger}_{\mathbf{k}\uparrow}\psi_{\mathbf{k}\downarrow}+e^{+im\phi}\psi^{\dagger}_{\mathbf{k}\downarrow}\psi_{\mathbf{k}\uparrow}.\end{aligned} \tag{14}$$

Band and pseudospin basis are related by:

$$\begin{aligned}\psi_{\mathbf{k}\sigma}&=\sum_{s}\langle\sigma|\mathbf{k}s\rangle\,\psi_{\mathbf{k}s},\\\begin{pmatrix}\psi_{\mathbf{k}\uparrow}\\\psi_{\mathbf{k}\downarrow}\end{pmatrix}&=\frac{1}{\sqrt{2}}\begin{pmatrix}e^{-im\phi/2}&e^{-im\phi/2}\\e^{+im\phi/2}&-e^{+im\phi/2}\end{pmatrix}\begin{pmatrix}\psi_{\mathbf{k}+}\\\psi_{\mathbf{k}-}\end{pmatrix}.\end{aligned} \tag{15}$$

Fermion bilinears transform as

$$\sum_{\sigma}\psi^{\dagger}_{\mathbf{k}_1\sigma}\psi_{\mathbf{k}_2\sigma}=\psi^{\dagger}_{\mathbf{k}_1 s_1}\sum_{s_1 s_2}\langle\mathbf{k}_1 s_1|\mathbf{k}_2 s_2\rangle\,\psi^{\dagger}_{\mathbf{k}_1 s_1}\psi_{\mathbf{k}_2 s_2}, \tag{16}$$

where

$$\langle\mathbf{k}_1 s_1|\mathbf{k}_2 s_2\rangle=\begin{pmatrix}\cos m\phi_{12}/2&i\sin m\phi_{12}/2\\i\sin m\phi_{12}/2&\cos m\phi_{12}/2\end{pmatrix}, \tag{17}$$

where ϕ_i is the polar angle of $\mathbf{k}_i$, and $\phi_{12}=\phi_1-\phi_2$. Therefore, the Hamiltonian in Eq. (1) of the Main text in the band basis is expressed as follows:

$$\begin{aligned}\mathcal{P}H\mathcal{P}&=\sum_{\mathbf{k}}E^{m}_{\mathbf{k}}\left(\psi^{\dagger}_{\mathbf{k}+}\psi_{\mathbf{k}+}-\psi^{\dagger}_{\mathbf{k}-}\psi_{\mathbf{k}-}\right)\\&-\sum_{\mathbf{k}_1\neq\mathbf{k}_2}\sum_{s_1 s_2}(T^{m}_{\mathbf{k}_1\mathbf{k}_2})^{s_1 s_2}\psi^{\dagger}_{\mathbf{k}_1 s_1}\psi_{\mathbf{k}_1\bar{s}_1}\psi^{\dagger}_{\mathbf{k}_2\bar{s}_2}\psi_{\mathbf{k}_2 s_2},\end{aligned} \tag{18}$$

where $E^{m}_{\mathbf{k}}=E_{\mathrm{UV}}(|\mathbf{k}|/\mathcal{K})^{m}+\Sigma^{m}_{\mathbf{k}}$ is the effective dispersion relation of the electrons, in which $\Sigma^{m}_{\mathbf{k}}$ is the self-energy

$$\Sigma^{m}_{\mathbf{k}}=\frac{1}{2A}\sum_{\mathbf{p}}V_{\mathbf{k}-\mathbf{p}}\cos(m\phi_{\mathbf{kp}}). \tag{19}$$

and $(T^{m})^{s_1 s_2}_{\mathbf{k}_1\mathbf{k}_2}$ is the interaction matrix in the band basis, given by:

$$T^{m}_{\mathbf{k}_1\mathbf{k}_2}=\frac{V_{\mathbf{k_1}-\mathbf{k_2}}}{4A}\begin{pmatrix}1+\cos(m\phi_{12})&1-\cos(m\phi_{12})\\1-\cos(m\phi_{12})&1+\cos(m\phi_{12})\end{pmatrix}. \tag{20}$$

B. Holstein-Primakoff expansion

We select the following spin basis

$$\mathbf{s_k} = -s^z_{\mathbf{k}}\hat{\mathbf{k}}_m + s^x_{\mathbf{k}}\hat{\mathbf{z}} + s^y_{\mathbf{k}}\hat{\boldsymbol{\phi}}_m, \tag{21}$$

which diagonalizes the kinetic term, and where $\hat{\mathbf{z}}$ is the normal axis to the layer and $\hat{\boldsymbol{\phi}}_m = \hat{\mathbf{z}} \times \hat{\mathbf{k}}_m = \big(-\sin(m\phi_m)\ \cos(m\phi_m)\big)$, and the exchange term is expanded as

$$\begin{aligned}
&\hat{\mathbf{s}}_{\mathbf{k}} \cdot\ \hat{\mathbf{s}}_{\mathbf{k}'} \\
&= \left(-\hat{s}^z_{\mathbf{k}_1}\hat{\mathbf{k}} + \hat{s}^x_{\mathbf{k}}\hat{\mathbf{z}} + \hat{s}^y_{\mathbf{k}}\hat{\boldsymbol{\varphi}}\right) \cdot \left(-\hat{s}^z_{\mathbf{k}'}\hat{\mathbf{k}}' + \hat{s}^x_{\mathbf{k}'}\hat{\mathbf{z}} + \hat{s}^y_{\mathbf{k}'}\hat{\boldsymbol{\varphi}}'\right) \\
&= (\hat{s}^z_{\mathbf{k}}\hat{s}^z_{\mathbf{k}'} + \hat{s}^y_{\mathbf{k}}\hat{s}^y_{\mathbf{k}'})\cos\phi_{\mathbf{kk}'} + \hat{s}^x_{\mathbf{k}}\hat{s}^x_{\mathbf{k}'} \\
&+\ (\hat{s}^y_{\mathbf{k}}\hat{s}^z_{\mathbf{k}'} - \hat{s}^z_{\mathbf{k}}\hat{s}^y_{\mathbf{k}'})\sin\phi_{\mathbf{kk}'}
\end{aligned} \tag{22}$$

with $\cos\phi_{\mathbf{kk}'} = \hat{\mathbf{k}}\cdot\hat{\mathbf{k}}' = \hat{\boldsymbol{\varphi}}\cdot\hat{\boldsymbol{\varphi}}'$. On this basis, the Hamiltonian can be expanded in a bosonic representation by means of the Holstein-Primakoff (HP) transformations ($S = 1/2$):

$$\begin{aligned}
s^z_{\mathbf{k}} &= 2\left(S - b^\dagger_{\mathbf{k}}b_{\mathbf{k}}\right) = 1 - 2b^\dagger_{\mathbf{k}}b_{\mathbf{k}}, \\
s^x_{\mathbf{k}} &\approx \sqrt{2S}\left(b_{\mathbf{k}} + b^\dagger_{\mathbf{k}}\right) = b_{\mathbf{k}} + b^\dagger_{\mathbf{k}}, \\
is^y_{\mathbf{k}} &\approx \sqrt{2S}\left(b_{\mathbf{k}} - b^\dagger_{\mathbf{k}}\right) = b_{\mathbf{k}} - b^\dagger_{\mathbf{k}}.
\end{aligned} \tag{23}$$

The term corresponding to the exchange coupling in Eq. (13) can be transformed into pairing and hopping terms of bosons up to bilinears:

$$\begin{aligned}
\mathbf{s_k}\cdot\mathbf{s}_{\mathbf{k}'} \approx &\left(1 + b^\dagger_{\mathbf{k}}b_{\mathbf{k}} + b^\dagger_{\mathbf{k}'}b_{\mathbf{k}'}\right)\cos\phi_{\mathbf{kk}'} \\
&+ \left(b^\dagger_{\mathbf{k}}b_{\mathbf{k}'} + b_{\mathbf{k}}b^\dagger_{\mathbf{k}'}\right)(1 + \cos\phi_{\mathbf{kk}'}) \\
&+ \left(b^\dagger_{\mathbf{k}}b^\dagger_{\mathbf{k}'} + b_{\mathbf{k}}b_{\mathbf{k}'}\right)(1 - \cos\phi_{\mathbf{kk}'}) \\
&+ i\left(b^\dagger_{\mathbf{k}} - b^\dagger_{\mathbf{k}'} - b_{\mathbf{k}} + b_{\mathbf{k}'}\right)\sin\phi_{\mathbf{kk}'}.
\end{aligned} \tag{24}$$

The resulting bosonic Hamiltonian after applying the HP transformations is:

$$\begin{aligned}
H_{HP} = &\sum_{\mathbf{k}} 2E_{\mathrm{UV}}\left(\frac{|\mathbf{k}|}{\mathcal{K}}\right)^m b^\dagger_{\mathbf{k}}b_{\mathbf{k}} + \sum_{\mathbf{k}\neq\mathbf{p}}\frac{V_{\mathbf{k}-\mathbf{p}}}{A}b^\dagger_{\mathbf{k}}b_{\mathbf{k}}\cos(m\phi_{\mathbf{kp}}) \\
&+ \sum_{\mathbf{k}\neq\mathbf{k}'}\frac{V_{\mathbf{k}-\mathbf{k}'}}{4A}(1 + \cos(m\phi_{\mathbf{k}_1\mathbf{k}_2}))\left(b^\dagger_{\mathbf{k}_1}b_{\mathbf{k}_2} + b_{\mathbf{k}_1}b^\dagger_{\mathbf{k}_2}\right) + \\
&+ \sum_{\mathbf{k}\neq\mathbf{k}'}\frac{V_{\mathbf{k}-\mathbf{k}'}}{4A}(1 - \cos(m\phi_{\mathbf{k}_1\mathbf{k}_2}))\left(b^\dagger_{\mathbf{k}_1}b^\dagger_{\mathbf{k}_2} + b_{\mathbf{k}_1}b_{\mathbf{k}_2}\right).
\end{aligned} \tag{25}$$

The first line contains the kinetic and self-energy terms. The second line can be viewed as boson hopping terms in the momentum lattice. The third line can be viewed as pairing terms which change the number of bosons. Lastly, by using the Bogoliubov basis given by

$$B^\dagger_{\mathbf{k}} = \begin{pmatrix} b^\dagger_{\mathbf{k}} & b_{\mathbf{k}} \end{pmatrix}, \tag{26}$$

the Hamiltonian can be expressed as

$$H_{HP} = \sum_{\mathbf{k}_1,\mathbf{k}_2} B^\dagger_{\mathbf{k}_1}H_{\mathbf{k}_1\mathbf{k}_2}B_{\mathbf{k}_2}, \tag{27}$$

with $B^\dagger_{\mathbf{k}} = \begin{pmatrix} b^\dagger_{\mathbf{k}} & b_{\mathbf{k}} \end{pmatrix}$, and

$$H_{\mathbf{k}_1\mathbf{k}_2} = \delta_{\mathbf{k}_1\mathbf{k}_2}\begin{pmatrix} 2E^m_{\mathbf{k}_1} & 0 \\ 0 & -2E^m_{\mathbf{k}_1} \end{pmatrix} - T^m_{\mathbf{k}_1\mathbf{k}_2}, \tag{28}$$

with $E_{\mathbf{k}} = v|\mathbf{k}| + \Sigma_{\mathbf{k}}$, $\Sigma_{\mathbf{k}} = \sum_{\mathbf{k}'} V_{\mathbf{k}-\mathbf{k}'}\cos(m\phi_{\mathbf{kk}'})/2A$ is the Hartree-Fock self-energy, $T_{\mathbf{kk}'}$ is

$$T_{\mathbf{kk}'} = \frac{V_{\mathbf{k}-\mathbf{k}'}}{4A}\begin{pmatrix} 1+\cos(m\phi_{\mathbf{kk}'}) & 1-\cos(m\phi_{\mathbf{kk}'}) \\ 1-\cos(m\phi_{\mathbf{kk}'}) & 1+\cos(m\phi_{\mathbf{kk}'}) \end{pmatrix}. \tag{29}$$

IV. HARTREE-FOCK SELF-ENERGY IN MULTILAYER GRAPHENE

The Hartree-Fock self-energy of the electrons and holes is given by

$$\Sigma^m(\mathbf{k}) = \int\frac{d^2\mathbf{p}}{(2\pi)^2}V(\mathbf{k}-\mathbf{p})\cos(m\phi_{\mathbf{kp}}), \tag{30}$$

The Fourier potential in (3) is then replaced in (30)

$$\Sigma^m(\mathbf{k}) = \frac{E_{\mathrm{UV}}}{\mathcal{K}^2}\int\frac{d^2\mathbf{p}}{(2\pi)^2}g_{\mathcal{K}}e^{-\frac{a^2_{\mathcal{K}}}{2}\left(\frac{\mathbf{k}-\mathbf{p}}{\mathcal{K}}\right)^2}\cos(m\phi_{\mathbf{kp}}), \tag{31}$$

In order to get an analytic expression for $\Sigma^m(\mathbf{k})$, it is defined the following integral as

$$I(k) = \int\frac{pdpd\phi}{(2\pi)^2}e^{-\left(\frac{k^2+p^2-2kp\cos\phi}{2}\right)}\cos(m\phi), \tag{32}$$

and, after substituting $x = a_{\mathcal{K}}p/\mathcal{K}$ and $y = a_{\mathcal{K}}k/\mathcal{K}$,

$$\begin{aligned}
I(k) &= \frac{\mathcal{K}^2}{a^2_{\mathcal{K}}}\int\frac{xdxd\phi}{(2\pi)^2}e^{-\left(\frac{x^2+y^2-2xy\cos\phi}{2}\right)}\cos(m\phi) \\
&= \frac{\mathcal{K}^2}{a^2_{\mathcal{K}}}\int\frac{xdx}{2\pi}e^{-\frac{x^2+y^2}{2}}\int\frac{d\phi}{2\pi}e^{xy\cos\phi}\cos(m\phi),
\end{aligned} \tag{33}$$

The polar integral is done using the Jacobi-Anger identity

$$e^{i\zeta\cos\phi} = \sum_{n=-\infty}^{+\infty}i^nJ_n(\zeta)e^{in\phi} = J_0(\zeta) + 2\sum_{n=1}^{\infty}i^nJ_n(\zeta)\cos(n\phi),$$

with imaginary argument $i\zeta = z$

$$e^{z\cos\phi} = \sum_{n=-\infty}^{+\infty}I_n(z)e^{in\phi} = J_0(z) + 2\sum_{n=1}^{\infty}I_n(z)\cos(n\phi), \tag{34}$$

so that

$$\begin{aligned}
&\int\frac{d\phi}{2\pi}e^{xy\cos(\phi)}\cos(m\phi)\\
&=\int\frac{d\phi}{2\pi}\left(I_0(xy)+2\sum_{n=1}^{\infty}I_n(xy)\cos(n\phi)\right)\cos(m\phi)\\
&=2\sum_{n=1}^{\infty}I_n(xy)\left(\int\frac{d\phi}{2\pi}\cos(n\phi)\cos(m\phi)\right)\\
&=\sum_{n=1}^{\infty}I_n(xy)\delta_{nm}=I_m(xy),
\end{aligned}\tag{35}$$

Substituting $I_m(xy)$ in the self-energy integral in Eq. (33) yields

$$\begin{aligned}
I(k)&=\frac{\mathcal{K}^2}{a_{\mathcal{K}}^2}\int\frac{xdx}{2\pi}e^{-\frac{x^2+y^2}{2}}\int\frac{d\phi}{2\pi}e^{xy\cos\phi}\cos(m\phi)\\
&=\frac{\mathcal{K}^2}{a_{\mathcal{K}}^2}\int\frac{xdx}{2\pi}e^{-\frac{x^2+y^2}{2}}I_m(xy)\\
&=\frac{\mathcal{K}^2}{a_{\mathcal{K}}^2}\frac{ye^{-\frac{y^2}{4}}}{4\sqrt{2\pi}}\left[I_{\frac{m-1}{2}}\left(\frac{y^2}{4}\right)+I_{\frac{m+1}{2}}\left(\frac{y^2}{4}\right)\right],
\end{aligned}\tag{36}$$

Finally, the self-energy of the m-layer graphene is then expressed as

$$\begin{aligned}
\Sigma^m(\mathbf{k})=&\frac{g_{\mathcal{K}}E_{\rm UV}}{8a_{\mathcal{K}}}\frac{ke^{-\frac{a_{\mathcal{K}}^2k^2}{4\mathcal{K}^2}}}{\mathcal{K}\sqrt{2\pi}}\times\\
&\times\left[I_{\frac{m-1}{2}}\left(\frac{a_{\mathcal{K}}^2k^2}{4\mathcal{K}^2}\right)+I_{\frac{m+1}{2}}\left(\frac{a_{\mathcal{K}}^2k^2}{4\mathcal{K}^2}\right)\right],
\end{aligned}\tag{37}$$

The two limit cases for large and small momenta are given by the following expressions:

$$\begin{aligned}
\lim_{k\to\infty}\Sigma^m(\mathbf{k})&=\frac{E_{\rm UV}}{4\pi a_{\mathcal{K}}^2}\\
\lim_{k\to 0}\Sigma^m(\mathbf{k})&=\frac{2^{-\frac{3n+4}{2}}E_{\rm UV}\left(\frac{a_{\mathcal{K}}k}{\mathcal{K}}\right)^n}{\sqrt{\pi}a_{\mathcal{K}}^2\Gamma\left(\frac{n+1}{2}\right)}
\end{aligned}\tag{38}$$

As special cases, the self-energy corresponding to any odd-layer and bilayer graphene are

$$\Sigma^n(\mathbf{k})=\frac{g_{\mathcal{K}}E_{\rm UV}}{8a_{\mathcal{K}}}\frac{ke^{-\frac{a_{\mathcal{K}}^2k^2}{4\mathcal{K}^2}}}{\mathcal{K}\sqrt{2\pi}}\left[I_n\left(\frac{a_{\mathcal{K}}^2k^2}{4\mathcal{K}^2}\right)+I_{n+1}\left(\frac{a_{\mathcal{K}}^2k^2}{4\mathcal{K}^2}\right)\right],\tag{39}$$

$$\begin{aligned}
\Sigma^2(\mathbf{k})=&\frac{g_{\mathcal{K}}E_{\rm UV}}{8a_{\mathcal{K}}}\frac{ke^{-\frac{a_{\mathcal{K}}^2k^2}{4\mathcal{K}^2}}}{\mathcal{K}\sqrt{2\pi}}\left[I_{\frac{1}{2}}\left(\frac{a_{\mathcal{K}}^2k^2}{4\mathcal{K}^2}\right)+I_{\frac{3}{2}}\left(\frac{a_{\mathcal{K}}^2k^2}{4\mathcal{K}^2}\right)\right]\\
=&\frac{g_{\mathcal{K}}E_{\rm UV}}{4\pi a_{\mathcal{K}}^2}\left[1-\frac{2\mathcal{K}^2}{a_{\mathcal{K}}^2k^2}\left(1-e^{-\frac{a_{\mathcal{K}}^2k^2}{2\mathcal{K}^2}}\right)\right],
\end{aligned}\tag{40}$$

where n is an odd integer (see the FIG. 3 for the cases of monolayer, bilayer and trilayer graphene). Their corresponding small-momentum regimes are described by

$$\begin{aligned}
\Sigma^1(\mathbf{k})&\approx\frac{g_{\mathcal{K}}E_{\rm UV}}{8\sqrt{2\pi}a_{\mathcal{K}}}\left(\frac{k}{\mathcal{K}}\right)+O(k^2),\\
\Sigma^2(\mathbf{k})&\approx\frac{g_{\mathcal{K}}E_{\rm UV}}{16\pi}\left(\frac{k}{\mathcal{K}}\right)^2+O(k^3),\\
\Sigma^3(\mathbf{k})&\approx\frac{a_{\mathcal{K}}E_{\rm UV}}{64\sqrt{2}\sqrt{\pi}}\left(\frac{k}{\mathcal{K}}\right)^3+O(k^4),
\end{aligned}\tag{41}$$

Notice that the dependence on $a_{\mathcal{K}}$ of the lowest-expansion-term coefficient for $\Sigma^1(\mathbf{k})$ is inverse to the dependence of $\Sigma^3(\mathbf{k})$. Even more, the lowest-expansion-term coefficient for $\Sigma^2(\mathbf{k})$ is independent of $a_{\mathcal{K}}$, as it is shown in FIG. 4.

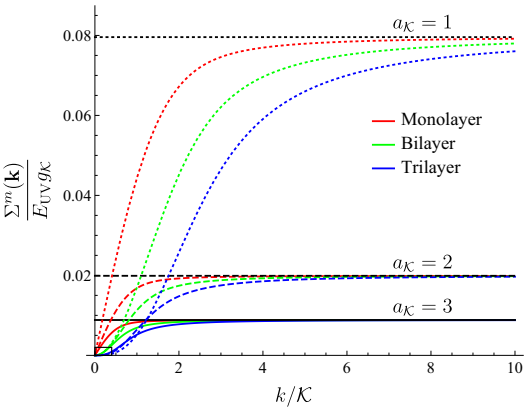

FIG. 3. Hartree-Fock self-energy $\Sigma^m(\mathbf{k})$ for monolayer ($m=1$, red), bilayer ($m=2$, green) and trilayer ($m=3$, blue) graphene. The dashing of the plots represent the value of the spreading parameter: $a_{\mathcal{K}}=1$ (dotted), $a_{\mathcal{K}}$ (dashed), and $a_{\mathcal{K}}=3$ (solid), while the horizontal black lines represent the asymptotic limit $\Sigma^m(\infty)$ the three values of $a_{\mathcal{K}}$. The little rectangle at the origin is zoomed in in FIG. 4.

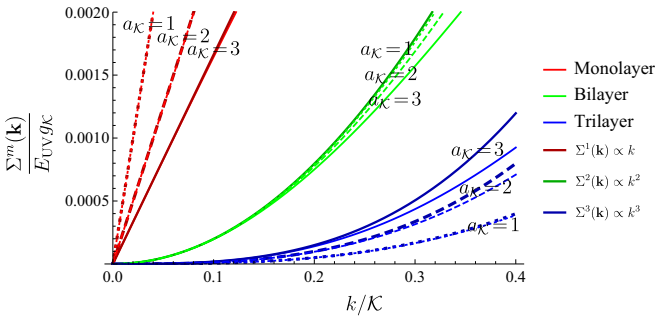

FIG. 4. Low-momentum limit for $\Sigma^m(\mathbf{k})$ in monolayer, bilayer and trilayer graphene. The legends are the same shown in FIG. 3 with the additional bolded curves representing the lowest-order expantion terms and labels of $a_{\mathcal{K}}$ to help with the interpretation of the plot. Notice that the low-momentum limit of $\Sigma^2(\mathbf{k})$ is independent of $a_{\mathcal{K}}$.

V. ANGULAR MOMENTUM CHANNELS AND PARAMETRIZATION OF THE RADIAL COORDINATE

In order to exploit the emergent rotational invariance in the thermodynamic limit, we use the following polar parametrization $\mathbf{z} = (k, \phi)$:

$$k_n = n\Delta k, \quad \phi_l = l\Delta\phi, \tag{42}$$

where (k_n, ϕ_l) are the polar coordinates of a given site in the polar momentum lattice, $\Delta k = \mathcal{K}/(N+1)$ with $n = 1, ..., N$, and $\Delta\phi = 2\pi/(2L+1)$ with $l = 0, ..., 2L$.

Because the Hamiltonian matrix $H_{\mathbf{k}\mathbf{k}'}$ that enters into the Hamiltonina H_{HP} in Eq. (27) of the main text only depends on the difference between the polar angles $\phi - \phi'$ we have conservation of the angular momentum ℓ of the bosons. Consequently, we perform Fourier transforms on the polar angle ϕ_l for the fields B^l_m and the matrix $H^{ll'}_{nn'}$

$$\begin{aligned} B^l_m &= \frac{1}{\sqrt{2L+1}} \sum_{\ell=-L}^{L} e^{-i\ell\phi_l} B^\ell_m, \\ H^{ll'}_{nn'} &= \sum_{\ell=-L}^{L} e^{-i\ell(\phi_l - \phi_{l'})} H^\ell_{mm'}, \end{aligned} \tag{43}$$

such that the total Bogoliubov Hamiltonian decomposes into a sum of decoupled angular mommentum channels, as follows:

$$H_{HP} = \sum_\ell H^\ell_{HP} = \sum_{nn'\ell} B^{\ell\dagger}_n H^\ell_{nn'} B^\ell_{n'}. \tag{44}$$

Therefore the problem reduces to a set of bosons moving in an effective one dimensional radial space of N sites for each angular momentum channel which in general needs to be solved numerically.

In that way, each dataset obtained from diagonalizing a $2N \times 2N$ matrix is labelled by the coupling constant $g_\mathcal{K}$ and spreading $a_\mathcal{K}$ of the Gaussian potential, the number of layers $m = 2$ fixed for bilayer graphene, the angular momentum ℓ and the number of sites in the radial coordinate N.

VI. NUMERICAL RESULTS

The solution of the system is found by using exact diagonalization on the $2N \times 2N$ matrix composed by the matrix elements of the Hamiltonian for the hopping $(b^\dagger_{k_1} b_{k_2})$ and pairing $(b_{k_1} b_{k_2}, b^\dagger_{k_1} b^\dagger_{k_2})$ terms. The parameters of the Hamiltonian are:

- Angular momentum $\ell = 0$, 1, 2, 3, 4, 5.
- Systen size $N = 100$, 200, 300, 400, 500.
- Coupling constant $a_\mathcal{K} = 0.01$, 0.02, 0.05, 0.10.

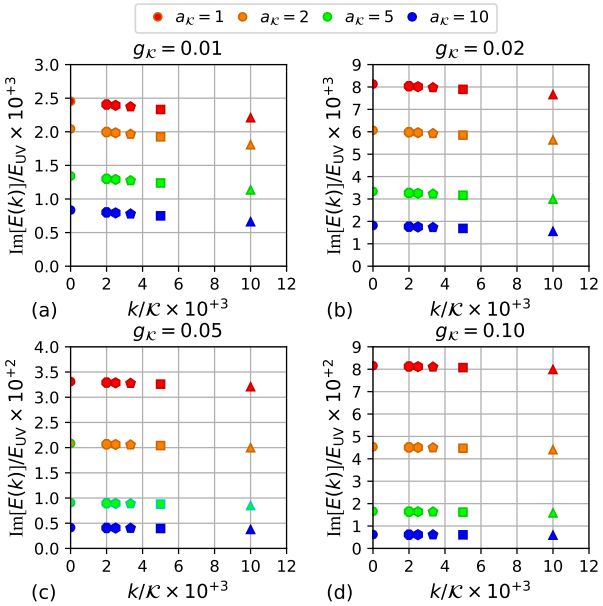

FIG. 5. △ ($N = 100$), □ ($N = 200$), ⬠ ($N = 300$), ⬡ ($N = 400$), and ◯ ($N = 500$). The extrapolation is ○ for $N \to \infty$.

- Reciprocal spreading $a_\mathcal{K} = 1$, 2, 5, 10.

and the UV-cutoff being set to the unity, $\mathcal{K} = 1$ and $E_{\mathrm{UV}} = 1$.

The Hamiltonian was diagonalized for each one of the 480 sets from the combinations of the parameters $\{\ell, N, g_\mathcal{K}, a_\mathcal{K}\}$, and then the energy spectra were examined looking for non-vanishing imaginary parts $\mathrm{Im}[E(k)]$ pointing out to an unstability in the modes of the system. The only two angular momentum channels that got non-vanishing imaginary parts in their eigenvalue spectra were $\ell = 0$ and $\ell = 2$, both showing only one eigenvalue with imaginary part (with the corresponding complementary eigenvalue with the opposite sign) at the smallest momentum,

$$\mathrm{Im}[E(k_{\min})] = \mathrm{Im}\left[E\left(\frac{\mathcal{K}}{N}\right)\right] \neq 0, \tag{45}$$

shown in the Figs. 5 and 6 for $\ell = 0$ and $\ell = 2$, respectively. Since the imaginary eigenvalues show a finite asympthotic trend when $k_{\min} \to 0$, i.e., $N \to \infty$, the five values obtain for each system size were useful to get the infinite size limit shown as the circles ○ in the foremen-tioned figures.

The main differences between $\ell = 0$ and $\ell = 2$ channels root on the relative size of its imaginary eigenvalues, being small for the latter channel, almost the half of those ones for the former channel. On the other hand, the channels show expected behaviors like the increase of $\mathrm{Im}[E(k_{\min})]$ for larger $g_\mathcal{K}$ meaning stronger interactions, and the suppression for larger $a_\mathcal{K}$ meaning a wider spreading of the potential, turning out in a weaker interaction and consequently, smaller values for $\mathrm{Im}[E(k_{\min})]$.

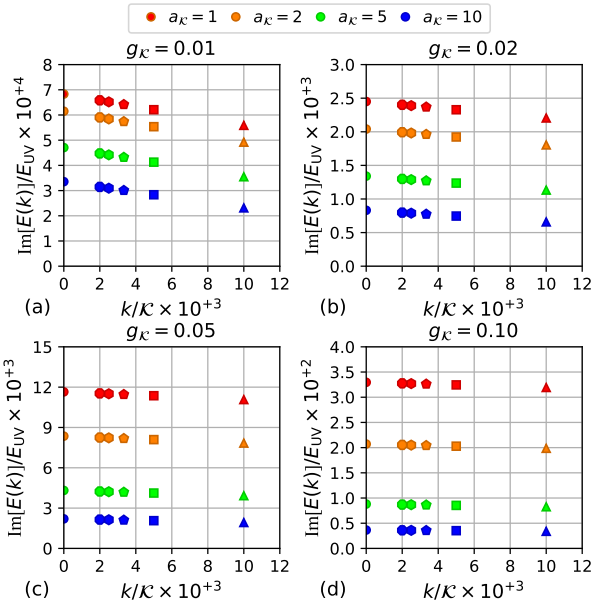

FIG. 6. $\triangle$ ($N=100$), $\square$ ($N=200$), $\pentagon$ ($N=300$), $\hexagon$ ($N=400$), and $\bigcirc$ ($N=500$). The extrapolation is $\bigcirc$ for $N\to\infty$.

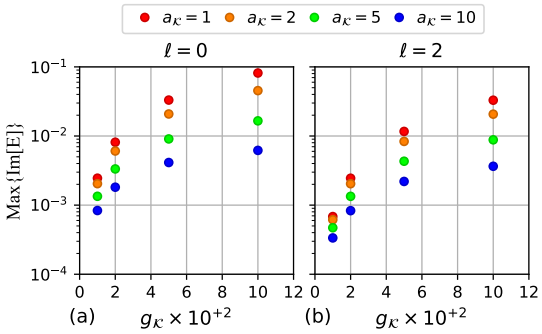

FIG. 7. $\triangle$ ($N=100$), $\square$ ($N=200$), $\pentagon$ ($N=300$), $\hexagon$ ($N=400$), and $\bigcirc$ ($N=500$). The extrapolation is $\bigcirc$ for $N\to\infty$.

The infinite size limits for $\mathrm{Im}[E(k_{\mathrm{min}}\to0)]$ are summarized in the Fig. 7 using the same color code and legends of Figs. 5 and 6.

VII. LOREM IPSUM

The Hamiltonian was diagonalized for each one of the 480 sets from the combinations of the parameters $\{\ell, N, g_\mathcal{K}, a_\mathcal{K}\}$, and then the energy spectra were examined looking for non-vanishing imaginary parts $\mathrm{Im}[E(k)]$ pointing out to an unstability in the modes of the system. The only two angular momentum channels that got non-vanishing imaginary parts in their eigenvalue spectra were $\ell=0$ and $\ell=2$, both showing only one eigenvalue with imaginary part (with the corresponding complementary eigenvalue with the opposite sign) at the smallest momentum,

$$\mathrm{Im}[E(k_{\mathrm{min}})]=\mathrm{Im}\left[E\left(\frac{\mathcal{K}}{N}\right)\right]\neq0, \tag{46}$$

shown in the Figs. 5 and 6 for $\ell=0$ and $\ell=2$, respectively. Since the imaginary eigenvalues show a finite asymptotic trend when $k_{\mathrm{min}}\to0$, i.e., $N\to\infty$, the five values obtain for each system size were useful to get the infinite size limit shown as the circles $\bigcirc$ in the foremention figures.

The main differences between $\ell=0$ and $\ell=2$ channels root on the relative size of its imaginary eigenvalues, being small for the latter channel, almost the half of those ones for the former channel. On the other hand, the channels show expected behaviors like the increase of $\mathrm{Im}[E(k_{\mathrm{min}})]$ for larger $g_\mathcal{K}$ meaning stronger interactions, and the suppression for larger $a_\mathcal{K}$ meaning a wider spreading of the potential, turning out in a weaker interaction and consequently, smaller values for $\mathrm{Im}[E(k_{\mathrm{min}})]$.

The Hamiltonian was diagonalized for each one of the 480 sets from the combinations of the parameters $\{\ell, N, g_\mathcal{K}, a_\mathcal{K}\}$, and then the energy spectra were examined looking for non-vanishing imaginary parts $\mathrm{Im}[E(k)]$ pointing out to an unstability in the modes of the system. The only two angular momentum channels that got non-vanishing imaginary parts in their eigenvalue spectra were $\ell=0$ and $\ell=2$, both showing only one eigenvalue with imaginary part (with the corresponding complementary eigenvalue with the opposite sign) at the smallest momentum,

$$\mathrm{Im}[E(k_{\mathrm{min}})]=\mathrm{Im}\left[E\left(\frac{\mathcal{K}}{N}\right)\right]\neq0, \tag{47}$$

shown in the Figs. 5 and 6 for $\ell=0$ and $\ell=2$, respectively. Since the imaginary eigenvalues show a finite asymptotic trend when $k_{\mathrm{min}}\to0$, i.e., $N\to\infty$, the five values obtain for each system size were useful to get the infinite size limit shown as the circles $\bigcirc$ in the foremention figures.

The main differences between $\ell=0$ and $\ell=2$ channels root on the relative size of its imaginary eigenvalues, being small for the latter channel, almost the half of those ones for the former channel. On the other hand, the channels show expected behaviors like the increase of $\mathrm{Im}[E(k_{\mathrm{min}})]$ for larger $g_\mathcal{K}$ meaning stronger interactions, and the suppression for larger $a_\mathcal{K}$ meaning a wider spreading of the potential, turning out in a weaker interaction and consequently, smaller values for $\mathrm{Im}[E(k_{\mathrm{min}})]$.

The Hamiltonian was diagonalized for each one of the 480 sets from the combinations of the parameters $\{\ell, N, g_\mathcal{K}, a_\mathcal{K}\}$, and then the energy spectra were examined looking for non-vanishing imaginary parts $\mathrm{Im}[E(k)]$ pointing out to an unstability in the modes of the system. The only two angular momentum channels that got non-vanishing imaginary parts in their eigenvalue spectra were $\ell=0$ and $\ell=2$, both showing only one eigenvalue with imaginary part (with the corresponding complementary eigenvalue with the opposite sign) at the smallest

momentum,

$$\mathrm{Im}[E(k_{\min})] = \mathrm{Im}\left[E\left(\frac{\mathcal{K}}{N}\right)\right] \neq 0, \tag{48}$$

shown in the Figs. 5 and 6 for $\ell = 0$ and $\ell = 2$, respectively. Since the imaginary eigenvalues show a finite asympthotic trend when $k_{\min} \to 0$, i.e., $N \to \infty$, the five values obtain for each system size were useful to get the infinite size limit shown as the circles $\bigcirc$ in the foremen-tioned figures.

The main differences between $\ell = 0$ and $\ell = 2$ channels root on the relative size of its imaginary eigenvalues, being small for the latter channel, almost the half of those ones for the former channel. On the other hand, the channels show expected behaviors like the increase of $\mathrm{Im}[E(k_{\min})]$ for larger $g_{\mathcal{K}}$ meaning stronger interactions, and the suppression for larger $a_{\mathcal{K}}$ meaning a wider spreading of the potential, turning out in a weaker interaction and consequently, smaller values for $\mathrm{Im}[E(k_{\min})]$.